Structural Studies on Ceramides as Lithiated Adducts by Low Energy Collisional-Activated Dissociation Tandem Mass Spectrometry with Electrospray Ionization

Fong-Fu Hsu and John Turk

Mass Spectrometry Resource, Division of Endocrinology, Diabetes, and Metabolism, Department of Medicine, Washington University School of Medicine, St. Louis, Missouri, USA

Mary E. Stewart and Donald T. Downing

The Marshall Dermatology Laboratories, Department of Dermatology, The University of Iowa, College of Medicine, Iowa City, Iowa, USA

We applied electrospray ionization (ESI) tandem quadrupole mass spectrometry to establish the fragmentation pathways of ceramides under low energy collisional-activated dissociation (CAD) by studying more than thirty compounds in nine subclasses. The product-ion spectra of the $[M + Li]^+$ ions of ceramides contain abundant fragment ions that identify the fatty acyl substituent and the long-chain base (LCB) of the molecules, and thus, the structure of ceramides can be easily determined. Fragment ions specific to each ceramide subclasses are also observed. These feature ions permit differentiation among different ceramide subclasses. The ion series arising from the classical C–C bond cleavages that were reported in the fast-atom bombardment (FAB)-high energy tandem mass spectrometry is not observable; however, the product-ion spectra contain multiple fragment ions informative for structural characterization and isomer identification. We also investigated the tandem mass spectra of the fragment ions generated by in-source CAD (pseudo-MS^3) and of the deuterium-labeling molecular species obtained by H/D exchange to support the ion structure assignments and the proposed fragmentation pathways that lead to the ion formation. (J Am Soc Mass Spectrom 2002, 13, 680–695) © 2002 American Society for Mass Spectrometry

Ceramides are *N*-acylated sphingoids (I), consisting of a long-chain aliphatic amino alcohol referred to as long-chain base (LCB), which are covalently linked to a fatty acyl chain via an amide linkage. The major LCB is a sphingosine (sphing-4-enine) (II), and smaller amounts of dihydrosphingosine (sphinganine) (III), phytosphingosine (4-hydroxysphinganine) (IV) also occur. The fatty acids of naturally occurring ceramides range in chain length from C_{16} to C_{26}, and may contain one or more double bonds/or hydroxyl substituents at C-2. Mammalian stratum corneum, however, contains more classes of ceramides than those made possible by various combinations of the classical building blocks. Pig stratum corneum, for example, contains two ceramides that have unusually long-chain ω-hydroxyacids. One of these ω-hydroxyceramides is solvent-extractable and has an additional fatty acid esterified to the ω-hydroxyl group [1], while the other ω-hydroxyceramide is protein-bound [2].

Human stratum corneum ceramides are similar to those in pig [3], except for the existence of a second protein-bound ceramide having a ω-hydroxyacid and a 6-hydroxysphing-4-enine (V) [4]. The identification of the second protein-bound ceramide in human epidermis was recently reported [5, 6]. These ceramides consist of a 6-hydroxysphing-4-enine bound to an ω-hydroxyacid (esterified to a fatty acid) and to an α-hydroxyacid, respectively.

Ceramides are also key compounds in the metabolism of sphingolipids and are emerging as important messengers for various cellular processes including cell cycle arrest, differentiation, apoptosis, senescence, and immune responses [7–13]. Because they have important biological functions, exact analysis of their molecular species and concentrations is crucial for elucidating their function and metabolism. Toward this goal, several methods including thin-layer, high performance liquid chromatography and mass spectrometry have been developed for the identification and quantitation of ceramides [14, 15]. Among them, tandem mass

Published online May 1, 2002

Address reprint requests to Dr. F.-F Hsu, Department of Internal Medicine, Washington University School of Medicine, 660 S. Euclid, Box 8127, St. Louis, MO 63110, USA. E-mail: fhsu@im.wustl.edu

1044-0305/02/$20.00
PII S1044-0305(02)00362-8

Received July 31, 2001
Revised February 1, 2002
Accepted February 4, 2002

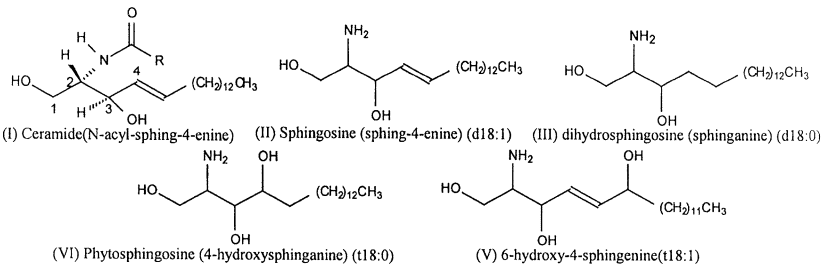

spectrometry with ESI has shown high sensitivity and selectivity for the analysis of ceramides without prior separation and derivatization [14–17].

Structural determination of ceramides as protonated or alkaline-metal adduct ions in the positive-ion mode or as their $[M - H]^-$ ions in the negative-ion mode using tandem mass spectrometry with FAB ionization was previously reported [18–20]. High energy CAD of the $[M + Li]^+$ ions of ceramides provides more structural information than CAD of either the $[M + H]^+$ or $[M - H]^-$ ions [18–20]. Low-energy product-ion spectra of the $[M + H]^+$ ions of ceramides produced by ESI are similar to those obtained by FAB, and only limited structural information is available [17–19]. Herein, we report a study of more than 30 ceramides in nine subclasses by CAD tandem quadrupole mass spectrometry with ESI. The low-energy product-ion spectra of the $[M + Li]^+$ ion of the ceramides contain abundant fragment ions that identify the structures of the fatty acyl substituent and the long-chain base of the molecule, and a more complete structural information than that observed by FAB CAD tandem sector mass spectrometry can be obtained.

Materials and Methods

Ceramide Standards and Their Abbreviations

The 6-hydroxy-4-sphingenine-containing ceramides in human skin were isolated as described [5, 6]. The structures of the ceramides were established by NMR spectroscopy as an acetylated derivative [5, 6]. The compounds, which were separated as an acetylated derivative by TLC, were deacetylated by adding 1 ml of 1M KOH in 95% methanol-5% water, heating to 60 °C for 60 min. After heating, 2 ml of chloroform and 0.6 ml of water (Folch extraction) were added, vortexed for 20 s, and centrifuged at 3000 × *g* for 5 min. The ceramides were recovered in the chloroform (lower) phase. The chloroform was blown to dryness under N_2, reconstituted in chloroform/methanol (1/4) and subjected to ESI/MS analysis.

The designation of ceramide is in the form of dLCB/FA, with d denoting a dihydroxy long chain base (LCB), namely, a 1,3-dihydroxyl-LCB, of which the 2-amino-octadec-4-ene-1,3-diol (sphing-4-enine) is designated as d18:1. The sphing-4-enine (sphingosine) may be substituted with an additional hydroxy group at C-6 to form a 6-hydroxysphing-4-enine, a trihydroxy long chain base, which is designated as t18:1. The 4-hydroxy sphinganine (phytosphingosine) LCB is designated as t18:0. FA refers to fatty acid, which is designated as nFA for a non-hydroxylated fatty acid, as hFA for an α-hydroxy fatty acid, and as ωFA for an ω-hydroxy fatty acid.

Mass Spectrometry

ESI/MS analyses were performed on a Finnigan (San Jose, CA) TSQ-7000 triple stage quadrupole mass spectrometer equipped with an electrospray ion source and controlled by Finnigan ICIS software operated on a DEC alpha station. Na^+ and K^+ were removed from samples if a high content was observed by ESI analysis. To remove them, samples were dissolved in chloroform and an aliquot (100 uL) of LiCl solution (0.6% aqueous) was added. After vortex, the solution was centrifuged for 5 min (3000 × *g*) and the organic layer was blown to dryness under a stream of nitrogen, and redissolved in chloroform/methanol (1/4), to a final concentration of 5 pmol/uL, which yields abundant Li^+ adduct ions upon ESI. Otherwise, standard ceramides and ceramide mixtures (5 pmol/uL) were prepared in chloroform/methanol (1/4), and methanolic LiCl (0.1 umol/uL) was added to give a final solution containing 1 nmol/uL Li^+. Samples were infused (1μL/min) into the ESI source, employing nitrogen as nebulizing gas. The electrospray needle was set at 4.5 kV and the skimmer was at ground potential. The heated capillary temperature was 250 °C. The precursor ion was selected in the first quadrupole (Q1) and collided with Ar (2.3 mtorr) in the rf-only second quadrupole (Q2) using a collision energy of 45–60 eV, and mass analyzed in the third quadrupole (Q3). For CAD tandem mass spectrometry of source-generated fragment ions (source CAD-MS^2), a voltage (30–60 V) was applied to the ion-transmission octapole to generate the primary fragment ions, which were then selected in the Q1 and collided with Ar (2.3 mtorr) in the Q2, using a collision energy of 25–35 eV. Both the Q1 and Q3 were tuned to unit mass resolution, and the mass spectra were obtained in the profile mode. Typically, a 1 min period of signal averaging was employed for scanned spectra, and 1 to 10 min was employed for tandem mass spectra.

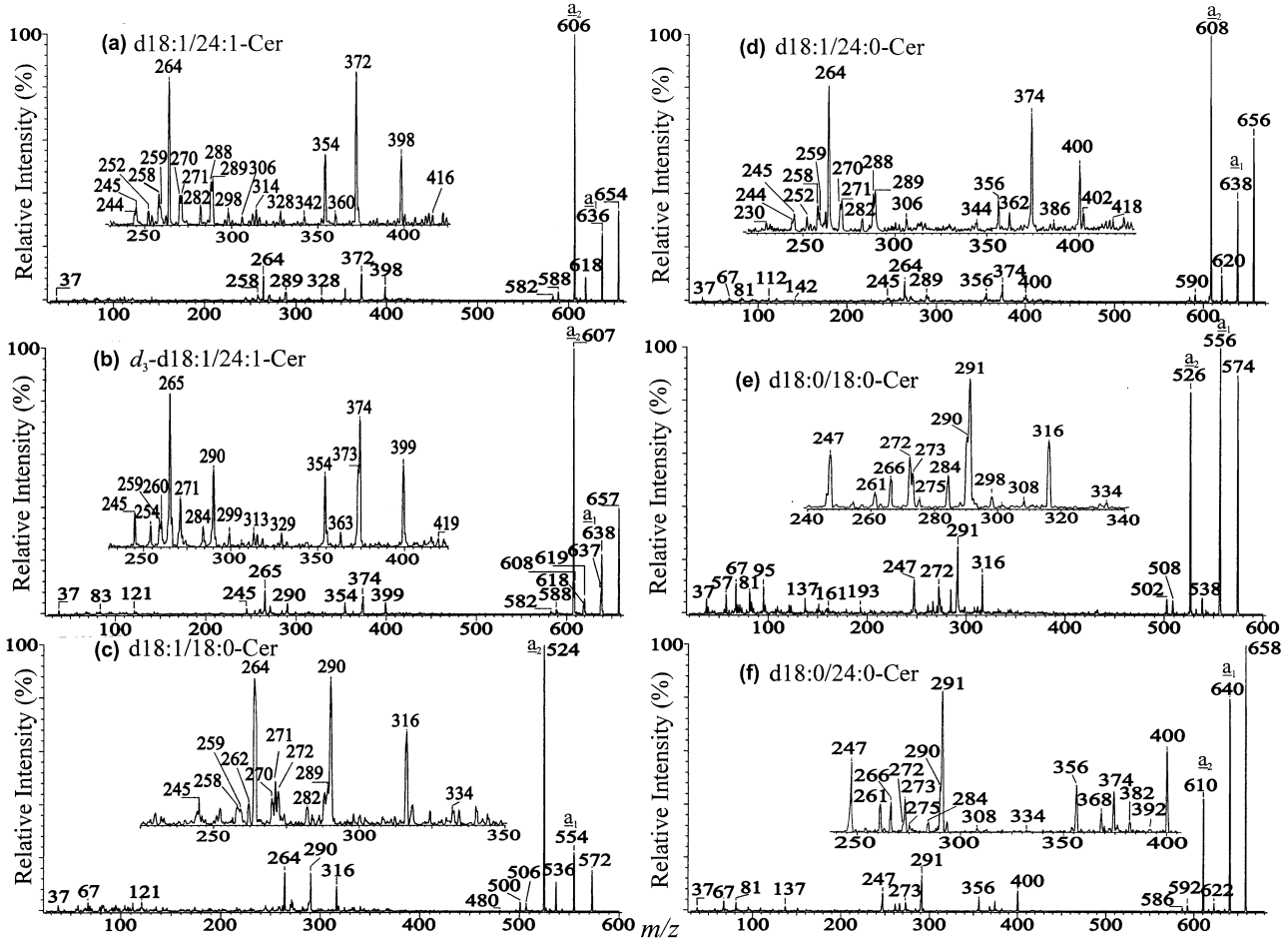

Figure 1. The ESI product-ion spectra of the $[M + Li]^+$ ions of (**a**) d18:1/24:1-Cer at *m/z* 654, (**b**) d_3-d18:1/24:1-Cer at *m/z* 657, (**c**) d18:1/18:0-Cer at *m/z* 572, (**d**) d18:1/24:0-Cer at *m/z* 656, (**e**) d18:0/18:0-Cer at *m/z* 574, and (**f**) d18:0/24:0-Cer at *m/z* 658.

Results and Discussion

In the presence of alkaline metal ions, ceramides yield abundant adduct ions ($[M + Alk]^+$, where Alk = Li, Na, K) upon ESI. However, only the lithiated adduct ion ($[M + Li]^+$) yields fragment ions that are informative for structural determination, similar to those obtained by high-energy tandem mass spectrometry [18–20]. The unique features of the $[M + Li]^+$ adduct ion applicable in the structural characterization using CAD tandem mass spectrometry were previously addressed [19, 21, 22]. The low-energy CAD tandem mass spectra of the $[M + Li]^+$ ions of ceramides also yield more structurally informative ions than those obtained from the $[M + H]^+$ ions [17] or from the $[M + Cl]^-$ ions in negative-ion mode [23]. The designation of the fragment ions previously used in the high energy CAD study [18–20] is not adopted because of the complexities of the ions observed.

N-Acylsphingosines

When subjected to CAD, the $[M + Li]^+$ ion of *N*-tetradodecenylsphingosine (d18:1/24:1-Cer) at *m/z* 654 yields a prominent ion at *m/z* 636 by loss of H_2O (Figure 1a). This is followed by further loss of H_2O or HCHO to give rise to ions at *m/z* 618 or 606, respectively. The formation of the *m/z* 636 ion by a water loss from *m/z* 654 may involve different mechanisms. This is revealed by the product-ion spectrum of the $[M + Li]^+$ ion of d_3-d18:1/24:1-Cer prepared by H–D exchange (Figure 1b). The spectrum contains the analogous ions at *m/z* 637 (loss of D_2O) and 638 (loss of DHO), indicating that the water loss can involve two or one exchangeable hydrogen. The *m/z* 636 ion successively yields a prominent ion at *m/z* 606 ($\underline{a}_2$) by loss of HCHO, or decomposes to a lithiated amide at *m/z* 372 ($\underline{d}_{1a}$, Scheme **1b**). The HCHO loss is consistent with the presence of the *m/z* 37 ion, which is a $[HCHO + Li]^+$ ion [24]. This process is confirmed by the product-ion spectrum of the *m/z* 636 ion (Figure 2a), generated by source CAD of d18:1/24:1-Cer at *m/z* 654. The *m/z* 372 ion can also arise from direct cleavage of the C2–N bond of the LCB (Scheme **1b**), as is revealed by the observation of the analogous ions of *m/z* 373 and 374 ($\underline{d}_{1a}$) in the product-ion spectrum of the lithiated d_3-d18:1/24:1-Cer (Figure 1b). The variation in the mass shifts of these two ions

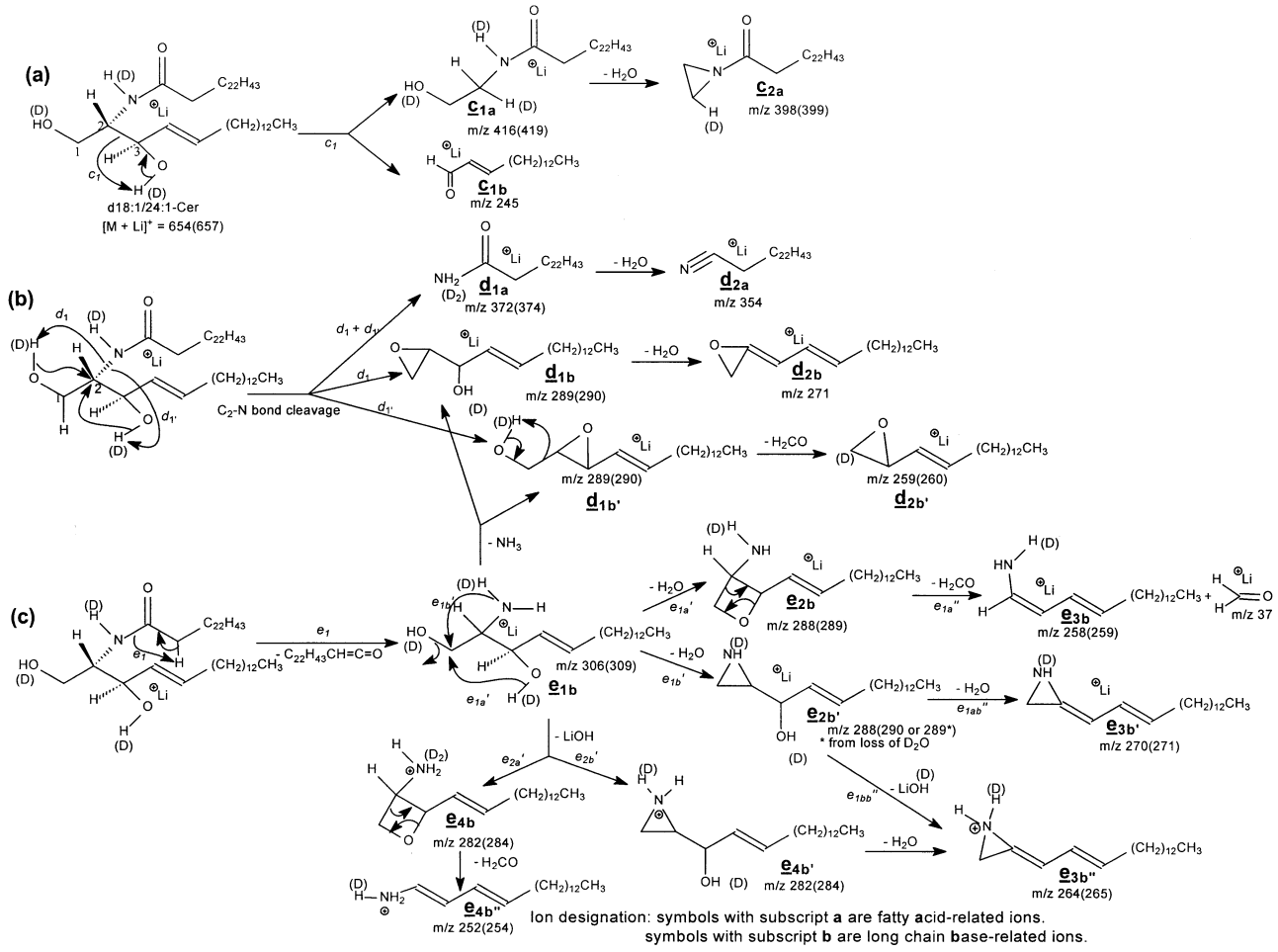

Scheme 1

arises from the exchangeable hydrogens. This result indicates that the two ions may derive from different pathways, or by H/D scrambling prior to fragmentation. The multiple pathways for formation of the *m/z* 636 ion are also supported by the product-ion spectra of the two isomeric ions of *m/z* 637 (Figure 2b) and 638 (Figure 2c), generated from source CAD of d_3-d18:1/24:1-Cer. The two spectra are readily distinguishable, consistent with the assignment that they are of isomers. The latter spectrum also contains more fragment ions than that of the former, indicating that the ions informative for the structural elucidation arise from further fragmentations of the *m/z* 638 ion rather than the *m/z* 637 ion. The summed product-ion spectrum of the two is similar to that arising from the *m/z* 636 ion (Figure 2a), generated by in-source CAD of the $[M + Li]^+$ ion of d18:1/24:1-Cer, and the abundance ratio of the *m/z* 638/637 ions also increases as the collision energy increases (data not shown). These results are consistent with the notion that the *m/z* 636 ion indeed arises via multiple pathways, and also consistent with the fragmentation pathways previously proposed for glycosphingolipids [24].

It appears that several cleavages involving the LCB chain have occurred. Although some of the ions arising from these cleavages are of low abundance and thus are of less diagnostic value, they appear to be precursors of many prominent ions that are informative for structural characterization. For example, the cleavage of the C2–C3 bond of the LCB (Scheme **1a**) results in a lithiated aldehyde ion at *m/z* 245 ($[CH_3(CH_2)_{12}CH{=}CHCHO + Li]^+$) ($\underline{c}_{1b}$). This cleavage also results in a low-abundance ion of *m/z* 416 ($\underline{c}_{1a}$), which leads to a prominent ion at *m/z* 398 ($\underline{c}_{2a}$) by loss of H_2O. The direct cleavage of the C2–N bond (Scheme **1b**) give rise to the *m/z* 372 ion ($\underline{d}_{1a}$), along with *m/z* 289, possibly a lithiated oxirane ($\underline{d}_{1b}$) or a lithiated epoxide ion ($\underline{d}_{1b'}$). The configurations for the *m/z* 289 ion are deduced by the fact that both a *m/z* 271 ($\underline{d}_{2b}$) and a *m/z* 259 ($\underline{d}_{2b'}$) ion were also observed in the spectrum. The former ion may arise from a H_2O loss from an oxirane intermediate of the *m/z* 289 ion ($\underline{d}_{1b'}$), which is primarily formed by the participation of the 1-hydroxy hydrogen for the C2–N bond cleavage (route d_1), whereas the *m/z* 259 ($\underline{d}_{2b'}$) ion is formed by loss of HCHO from a lithiated epoxide intermediate of *m/z* 289 ($\underline{d}_{1b'}$), which arises from the same cleavage involving the 3-hydroxy hydrogen (route $d_{1'}$) of the

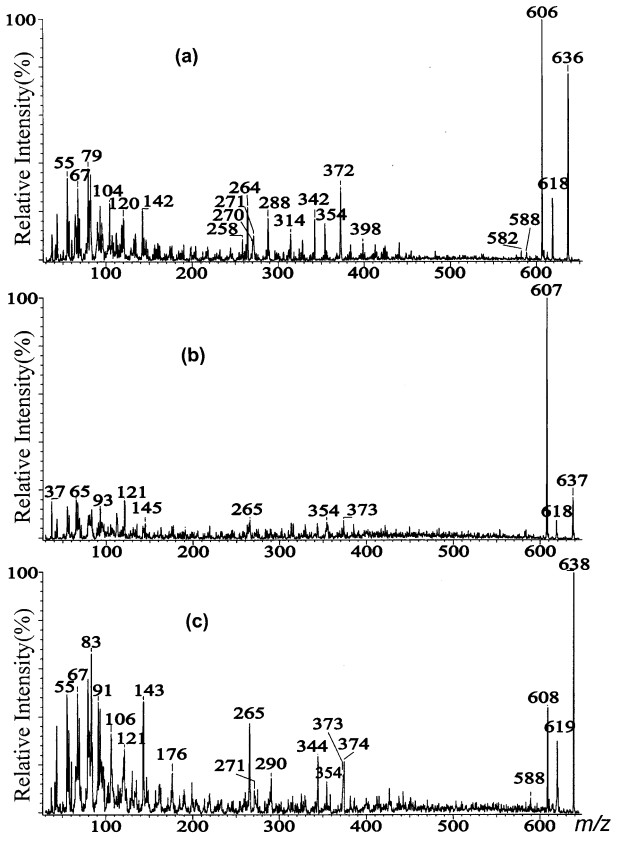

Figure 2. The product-ion spectra (**a**) of the *m/z* 636 ion, generated from source CAD of the $[M + Li]^+$ ions of d18:1/24:1-Cer, (**b**) of the *m/z* 637 and (**c**) of the *m/z* 638 ion, generated from source CAD of d_3-d18:1/24:1-Cer.

LCB. The *m/z* 372 ion may also undergo a H_2O loss to a *m/z* 354 ion ($\underline{d}_{2a}$).

The elimination of the fatty acyl group as a ketene (loss of $C_{22}H_{43}CH{=}C{=}O$) (Scheme **1c**) from the *m/z* 654 ion results in a low-abundance ion of *m/z* 306 ($\underline{e}_{1b}$), which becomes the most prominent in the product-ion spectra of the *N*-α-hydroxylsphingosines (discussed later). The *m/z* 306 ion is a lithiated sphingosine, which appears to be the precursor ion leading to the *m/z* 288 or 289 ion by a H_2O or NH_3 loss, respectively. The *m/z* 306 ion may also yield the protonated ion species of *m/z* 282 ($\underline{e}_{4b} + \underline{e}_{4b'}$) via loss of LiOH. The H_2O loss from *m/z* 306 may involve two pathways leading to a lithiated oxetane ($\underline{e}_{2b}$) or a lithiated aziridine ($\underline{e}_{2b'}$) ion of *m/z* 288. The oxetane intermediate of *m/z* 288 ($\underline{e}_{2b}$) arises from the water loss that involves the 3-hydroxyl hydrogen of the LCB (route e_{1a}) and further dissociates to a conjugated diene at *m/z* 258 ($\underline{e}_{3b}$) or to a lithiated HCHO ion at *m/z* 37, whereas the aziridine intermediate of *m/z* 288 ion ($\underline{e}_{2b'}$) arises from a ring closure by the water loss involving the amide hydrogen (route $e_{1b'}$). This is followed by another water or LiOH loss to yield a *m/z* 270 ($\underline{e}_{3b'}$) (route $e_{1ab''}$) or 264 ion ($\underline{e}_{3b''}$) (route $e_{1bb''}$). The similar fragmentation pathways can be reasoned for the formation of the protonated oxetane ($\underline{e}_{4b}$) (route $e_{2a'}$) or aziridine ($\underline{e}_{4b'}$) (route $e_{2b'}$) ion of the *m/z* 282 ion arising from a LiOH loss from the *m/z* 306 ion. These pathways are also consistent with the observation of the prominent ions of *m/z* 252 ($\underline{e}_{4b''}$) and 264 ($\underline{e}_{3b''}$) arising from *m/z* 282 by loss of HCHO and H_2O, respectively. The above fragmentation pathways are confirmed by the product-ion spectra of the *m/z* 306 (Figure 3a) and *m/z* 288 (Figure 3b) ions, generated by source CAD of the

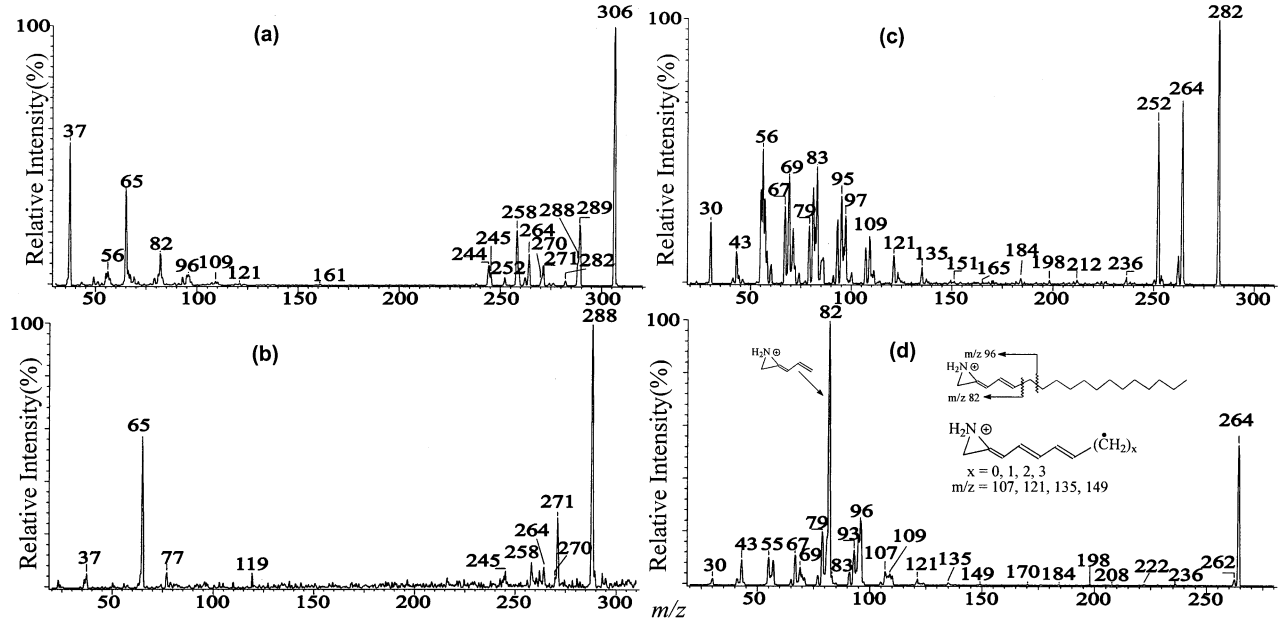

Figure 3. The product-ion spectra of (**a**) the *m/z* 306 ion, (**b**) the *m/z* 288 ion, (**c**) the *m/z* 282 ion, and (**d**) the *m/z* 264 ion. The ions at *m/z* 306 and 288 were generated from source CAD of the $[M + Li]^+$ ions of d18:1/24:1-Cer at *m/z* 654. The *m/z* 282 and 264 ions were generated from source CAD of the $[M + H]^+$ ion of d18:1/24:1-Cer at *m/z* 648.

Table 1. Major fragment ions observed for various ceramide standards

Ceramide species			Fragment ions from CAD of $[M + Li]^+$															
			common ions (*m/z*)			FA ions (*m/z*)							LCB ions (*m/z*)					
$[M + Li]^+$	Fatty acid	LCB	$\underline{a}_1$	$\underline{a}_2(a_1\text{-}30)$	$\underline{a}_1\text{-}18$	$\underline{c}_{2a}$	$\underline{c}_{3a'}$[d]	$\underline{b}_{1a}$[d]	$\underline{b}_{2a}$[d]	$\underline{g}_{3a}$[d]	$\underline{d}_{1a}$	$\underline{d}_{2a}$[d]	$\underline{d}_{3b}$	$\underline{e}_{1b}$	$\underline{e}_{2b} + \underline{e}_{2b'}$	$\underline{e}_{3b'}$	$\underline{e}_{3b''}$	$\underline{f}_{3b'}$
656	24:0	d18:1	638	608	620	400[d]					374[d]	356			288[d]	270[d]	264[d]	
654	24:1	d18:1	636	606	618	398[d]					372[d]	354			288[d]	270[d]	264[d]	
657	24:1	d_3-d18:1	638,637	607	618,619	399[d]					374,375[d]	354			290[d]	271[d]	265[d]	
432	8:0	d18:1	414	384	396	176[d]					150[d]	132			288[d]	270[d]	264[d]	
544	16:0	d18:1	526	496	508	288[d]					262[d]	244			288[d]	270[d]	264[d]	
572	18:0	d18:1	554	524	536	316[d]					290[d]	272			288[d]	270[d]	264[d]	
658	24:0	d18:0	640	610	622	400[d]					374[d]	356	275	308	290[d]	272	266[d]	
661	24:0	d_3-d18:0	641,642	611	622,623	401[d]					375,376[d]	356	276	311	291[d]	273	267[d]	
574	18:0	d18:0	556	526	538	316[d]					290[d]	272	275	308	290[d]	272	266[d]	
672	h24:0	d18:1	654	624	636	416	345				390		273	306	288[d]	270	264	298[d]
676	d_1-h24:0	d_3-d18:1	656,657	626	639,638	418	345				392,393		274	310	290[d]	271	266	299[d]
670	h24:1	d18:1	652	622	634	414	343				388		273	306[d]	288[d]	270	264	298[d]
532	h16:0	d16:1	514	484	496	304	233				278		245	278[d]	260[d]	242	236	270[d]
546	h16:0	d17:1	528	498	510	304	233				278		259	292[d]	274[d]	256	250	284[d]
560	h16:0	d18:1	542	512	524	304	233				278		273	306[d]	288[d]	270	264	298[d]
562	h16:0	d18:0	544	514	526	304	233				278		275[d]	308[d]	290[d]	272		300
590	h18:0	d18:0	572	542	554	332	261				306		275[d]	308[d]	290[d]	272		300
548	h16:0	d17:0	530	500	512	304	233				278		261[d]	294[d]	276[d]	258		286
756	ω30:0	d18:1	738	708	720	500[d]					474[d]	456			288	270	264	
784	ω30:0	d20:1	766	736	748	500[d]					474[d]	456			316	298	292	
	ω32:0	d18:1	766	736	748	500[d]					502[d]	484			288	270	264	
578	h16:0	t18:0	560	530	542	304	233				278		291[d]	324[d]	306[d]	288		316
564	h16:0	t17:0	546	516	528	304	233				278		277[d]	310[d]	292[d]	274		302
800	ω30:0	t20:1	782	752	764	500[d]				526	474[d]	456	317		332	314[d]	308	
	ω32:0	t18:1	782	752	764	528[d]				554	502[d]	484	289		304	*286[d]	**280	
772	ω30:0	t18:1	754	724	736	500[d]				526	474[d]	456	289		304	*286[d]	**280	
744	ω28:0	t18:1	726	696	708	472[d]				498	446[d]	428	289		304	*286[d]	**280	
674	24:0	t18:0	656	626	638	400[d]		428	416		374[d]	356	291		306	288[d]		
	25:0	t17:0	656	626	638	414		442	430		388[d]	370	277		292	274		
	26:0	t16:0	656	626	638	428		456	444		402[d]	384	263		278	260		
660	24:0	t17:0	642	612	624	400		428	416		374[d]	356	277		292	274		
702	26:0	t18:0	684	654	666	428		456	444		402[d]	384	291		306	288		
688	h24:0	t18:1	670	640	652	416	345				390		289[d]	322[d]	304[d]	286[d]		314
716	h26:0	t18:1	698	668	680	444	373				418		289[d]	322[d]	304[d]	286[d]		314

[d]diagnostic ions.
*also a $e_{5b'}$ ion.
**also a $e_{5b''}$ ion.

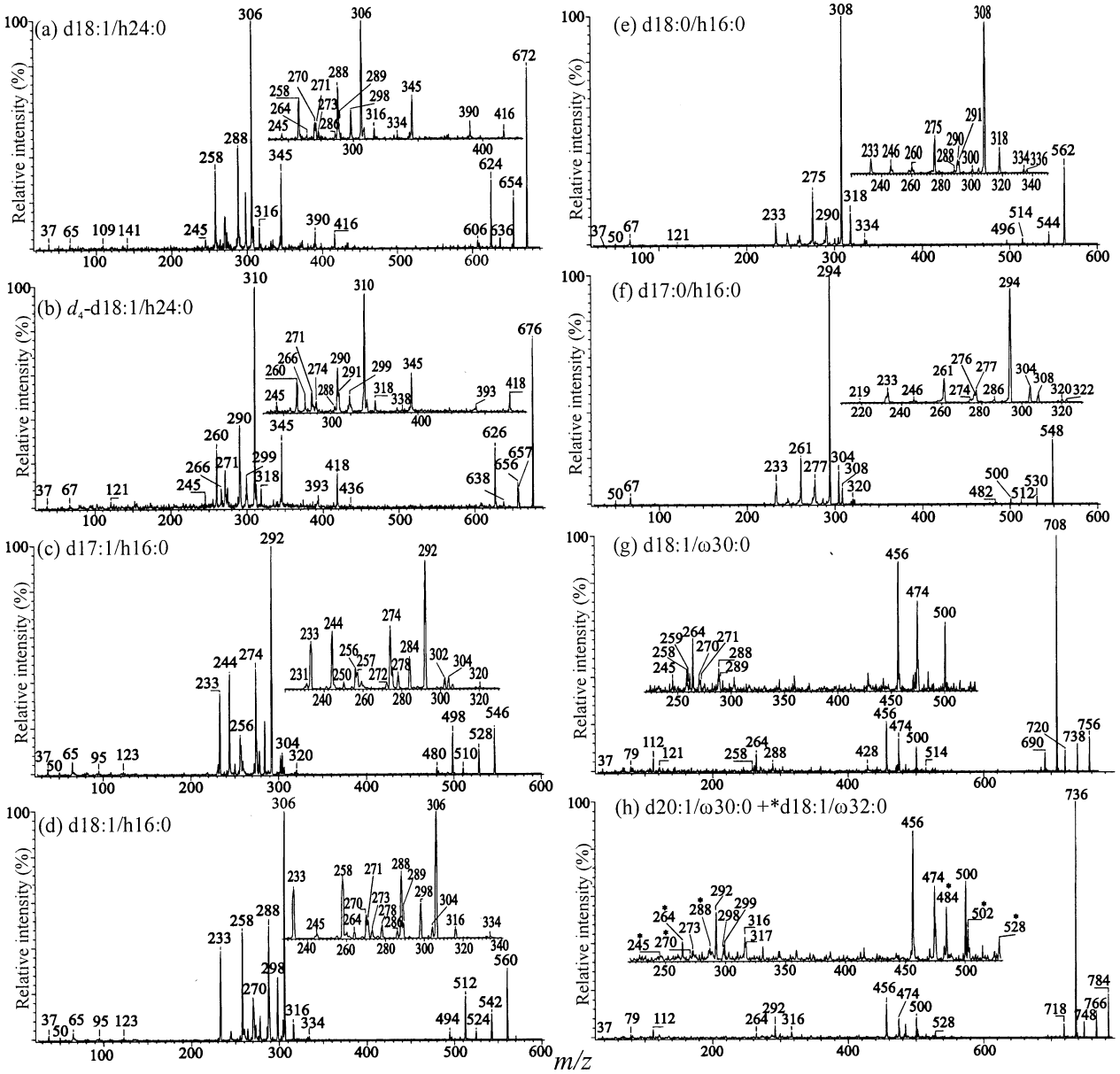

Figure 4. The product-ion spectra of the $[M + Li]^+$ ion of (**a**) d18:1/h24:0-Cer at *m/z* 672, (**b**) d_4-d18:1/h24:0-Cer at *m/z* 676, (**c**) d17:1/h16:0-Cer at *m/z* 546, (**d**) d18:1/h16:0-Cer at *m/z* 560, (**e**) d18:0/h16:0-Cer at *m/z* 562, (**f**) d17:0/h16:0-Cer at *m/z* 548, (**g**) d18:1/ω30:0-Cer at *m/z* 756, and of (**h**) (d20:1/ω30:0 + *d18:1/ω32:0)-Cer at *m/z* 784. The fragmentations of the ceramides are facilitated by the presence of the α-hydroxyl group of the fatty acyl chain, regardless of the LCB (panels **a**–**f**), and not affected by the ω-hydroxyl group (panels **g**, **h**). The analogous ions arising from the second isomer in panel H are marked with an asterisk.

lithiated 18:1/24:1-Cer at *m/z* 654, and of *m/z* 282 ion (Figure 3c), generated by source CAD of the protonated 18:1/24:1-Cer at *m/z* 648.

The *m/z* 264 ($\underline{e}_{3b''}$) is the most prominent ion observed for the $[M + H]^+$ ions of d18:1/nFA-Cer after CAD [17, 21]. We speculate that the *m/z* 264 is a conjugated aziridine ion ($\underline{e}_{3b''}$, Scheme **1c**). This is based on the findings that the product-ion spectrum of the *m/z* 264 ion (Figure 3d) contains a prominent ion at *m/z* 82, possibly corresponding to a stable protonated aziridine. However, a more detailed study is required to prove the suggested structure. The formation of both an oxetane and aziridine isomeric ions by a ring closure as proposed in Scheme **1** is also reasoned by the fact that the exchangeable hydrogens rather than the C–H hydrogens have been eliminated for the H_2O loss. This H_2O loss is confirmed by the product-ion spectra of the H–D exchanged analogs (Scheme **1**, the *m/z* values observed for the deuterium-labeling compound are shown in parentheses).

Since the major ions at *m/z* 264 ($\underline{e}_{3b''}$) and 372 ($\underline{d}_{1a}$) respectively reflect the long-chain base and fatty acid

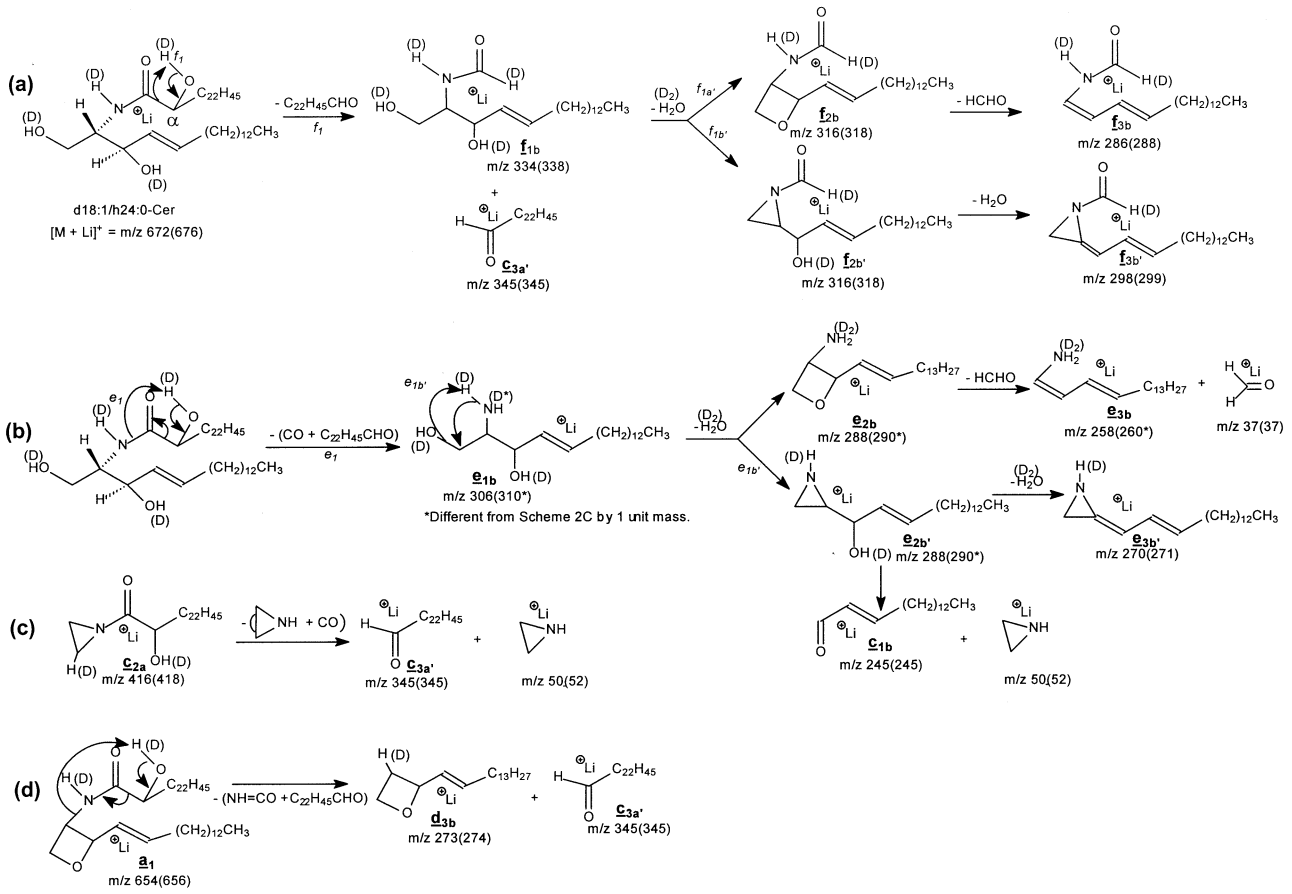

Ion designation: symbols with subscript **a** are fatty **a**cid-related ions.
symbols with subscript **b** are long chain **b**ase-related ions.

Scheme 2

moieties of the molecule, the structure of the compound can be easily identified. In addition, the presence of the ions at *m/z* 398 ($\underline{c}_{2a}$) and 354 ($\underline{d}_{2a}$) in the spectrum confirms that the fatty acid substituent of the molecule is 24:1, whereas the d18:1-LCB can be confirmed by the presence of the ions at *m/z* 245 ($\underline{c}_{1b}$), 289 ($\underline{d}_{1b}$ + $\underline{d}_{1b'}$), 271 ($\underline{d}_{2b}$), 288 ($\underline{e}_{2b}$ + $\underline{e}_{2b'}$), 258 ($\underline{e}_{3b}$), 259 ($\underline{d}_{2b'}$), 270 ($\underline{e}_{3b'}$), and 282 ($\underline{e}_{4b'}$). A similar pattern of the ions was also observed for the $[M + Li]^+$ ions of d18:1/18:0-Cer (*m/z* 572, Figure 1c), d18:1/24:0-Cer (*m/z* 656, Figure 1d), d18:0/18:0-Cer (*m/z* 574, Figure 1e), and of d18:0/24:0-Cer (*m/z* 658, Figure 1f). Figure 1c and e show abundant ions at *m/z* 316 ($\underline{c}_{2a}$), 290 ($\underline{d}_{1a}$), and 272 ($\underline{d}_{2a}$) that reflect the stearic acid moiety of the molecules, and Figure 1d and f contain ions at *m/z* 400 ($\underline{c}_{2a}$), 374 ($\underline{d}_{1a}$), and 356 ($\underline{d}_{2a}$), reflecting the tetracosanoic acid. The identity of the LCBs for both the lithiated d18:1/18:0-Cer (Figure 1c) and d18:1/24:0-Cer (Figure 1d) is reflected by the prominent ions at *m/z* 264 ($\underline{e}_{3b''}$), together with the aforementioned ions that are characteristic of d18:1-LCB, whereas the d18:0-LCB for both the lithiated d18:0/18:0-Cer (Figure 1e) and d18:0/24:0-Cer (Figure 1f) is identified by the abundant ion at *m/z* 291($\underline{d}_{1b}$ + $\underline{d}_{1b'}$) together with ions at *m/z* 266 ($\underline{e}_{3b''}$), *m/z* 247 ($\underline{c}_{1b}$), 273 ($\underline{d}_{2b}$), 308 ($\underline{e}_{1b}$), 290 ($\underline{e}_{2b}$ + $\underline{e}_{2b'}$), 272 ($\underline{e}_{3b'}$), 261 ($\underline{d}_{2b'}$), and 284 ($\underline{e}_{4b'}$), which are two units higher than the analogous ions observed for d18:1-LCB.

The apparent distinction of the product-ion spectra of d18:0/nFA-Cer from that of d18:1/nFA-Cer is that the $[M + Li - H_2O - HCHO]^+$ ($\underline{a}_2$) ions are the most prominent for d18:1/nFA-Cer (Figure a, b, c, and d), while the $[M + Li - H_2O]^+$ ($\underline{a}_1$) ions are the most abundant for d18:0/nFA-Cer (Figure 1e and f) (Table 1), when obtained at the same collision energy (50 eV). The saturation of the LCB bond also results in the decline of the $e_{3b''}$ ion at *m/z* 266 and the $\underline{e}_{3b'}$ ion at *m/z* 272 (the *m/z* 272 ion in Figure 1e is also a $\underline{d}_{2a}$ ion), and accounts for the absence of the $\underline{e}_{3b}$ ion of *m/z* 260 for d18:0/nFA-Cer. This is attributable to the fact that ions of $\underline{a}_2$, *m/z* 272 ($\underline{e}_{3b'}$), *m/z* 266 ($\underline{e}_{3b''}$), and *m/z* 260 ($\underline{e}_{3b}$) arising from d18:0/FA-Cer are less conjugated and less stable than the corresponding ions of a_2, the *m/z* 270 ($\underline{e}_{3b'}$), 264 ($\underline{e}_{3b''}$), and 258 ($\underline{e}_{3b}$), arising from d18:1/nFA-Cer (panel a, b, c, and d). The disparities of the product-ion spectra among the d18:1- and d18:0-LCB subclasses of glycosphingolipids were previously reported and have the implication for differentiation of cerebroside isomers [24]. Another feature in the product-ion spectra of the

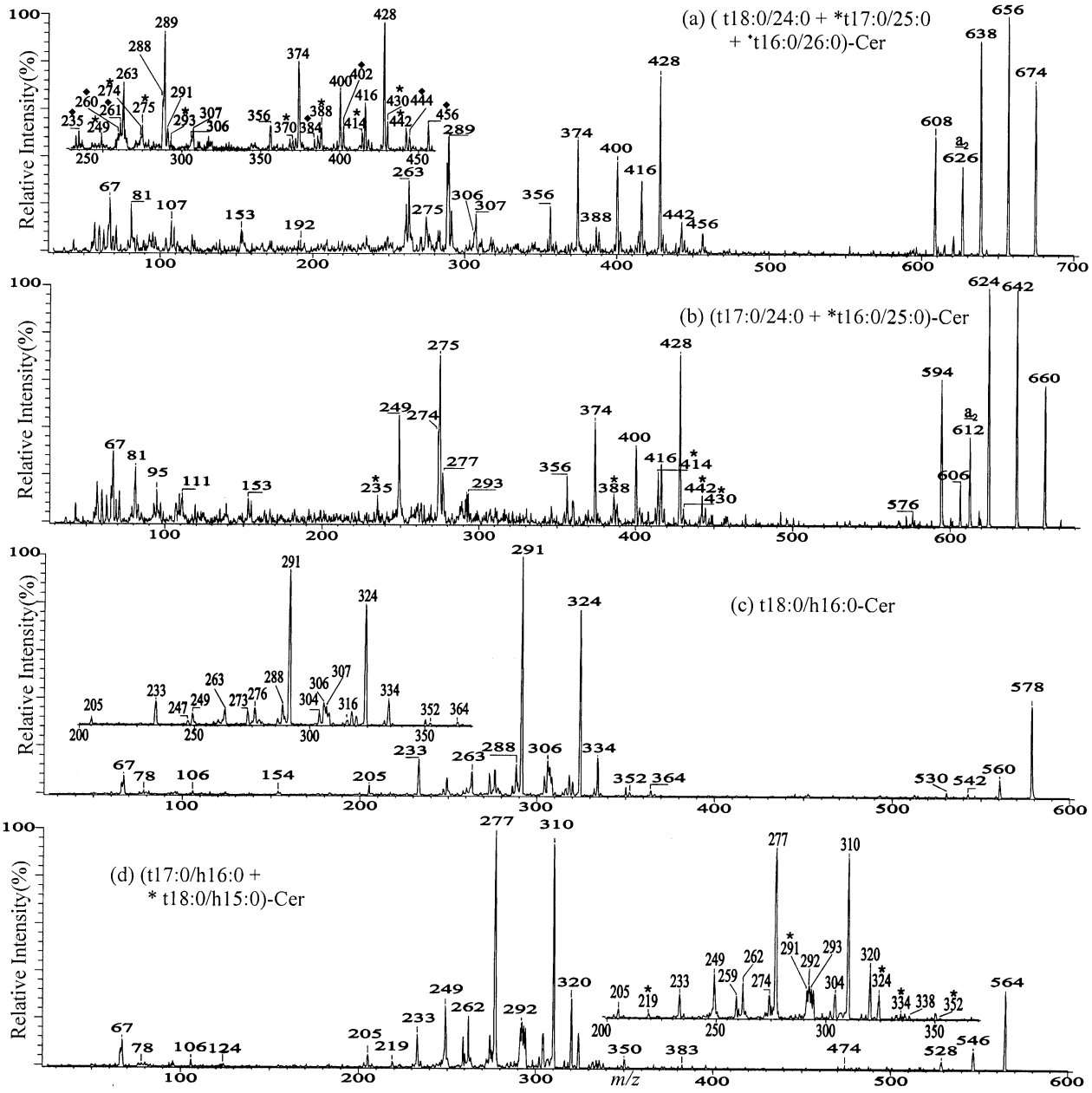

Figure 5. The product-ion spectra of the $[M + Li]^+$ ions of (**a**) (t18:0/24:0 + *t17:0/25:0 + ◆t16:0/26:0)-Cer at *m/z* 674, (**b**) (t17:0/24:0 + *t16:0/25:0)-Cer at *m/z* 660, (**c**) t18:0/h16:0-Cer at *m/z* 578, and (**d**) (t17:0/h16:0 + *t18:0/h15:0)-Cer at *m/z* 564. Ions marked with an asterisk and a superior filled diamond are the analogous ions arising from the second and the third isomer, respectively.

$[M + Li]^+$ ions of d18:0/nFA-Cer is that the *m/z* 291 ion ($\underline{d}_{1b} + \underline{d}_{1b'}$) is of abundance and a protonated amide ion at 284 ($C_{17}H_{35}CONH_3^+$) and *m/z* 368 ($C_{23}H_{47}CONH_3^+$) is present, respectively, in the spectrum of d18:0/18:0-Cer (Figure 1e) and of d18:0/24:0-Cer (Figure 1f). This may be attributable to the fact that the ketene loss (Scheme **1c**) to yield a stable conjugated ion species is a more favorable fragmentation pathway than the C2–N bond cleavage (Scheme **1b**) for d18:1/nFA-Cer. However, this pathway becomes less favorable for the lithiated d18:0/nFA-Cer, in which the analogous ions that are less conjugated are formed. As a result, the C2–N bond cleavage pathway leading to the formation of the *m/z* 291 ion prevails.

N-α-hydroxyacylsphing-4-enines (d18:1/hFA-Cer) and N-ω-hydroxyacylsphing-4-enines (d18:1/ωFA-Cer)

Under the same collision energy, the lithiated *N-α*-hydroxyacylsphingenines undergo more extensive fragmentations than the corresponding ions arising from *N*-acylsphingenines. As illustrated in Figure 4a, the

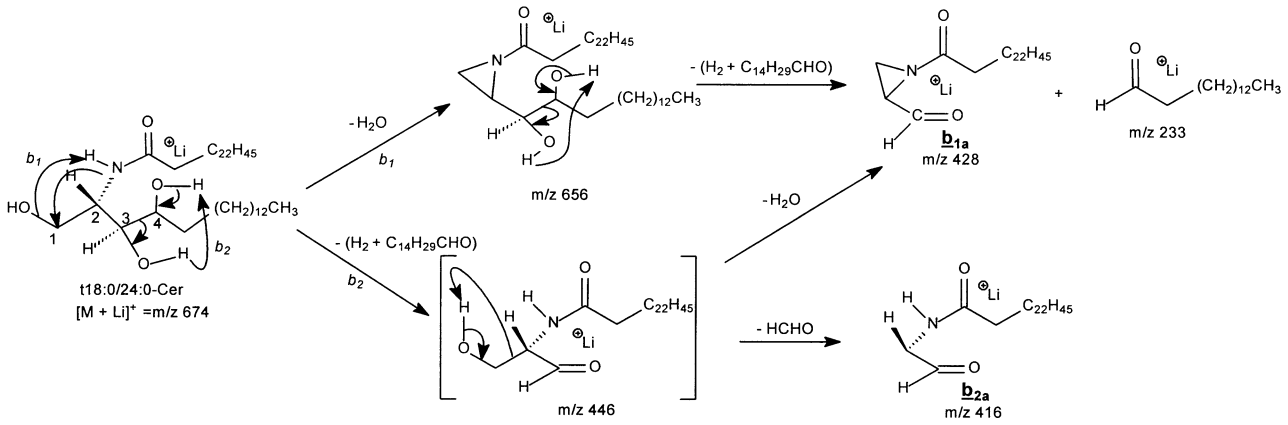

Scheme 3

product-ion spectrum of the lithiated d18:1/h24:0-Cer at *m/z* 672 contains common ions at *m/z* 654 ($[M + Li - H_2O]^+$) ($\underline{a}_1$), 636 ($[M + Li - 2H_2O]^+$) ($\underline{a}_1 - H_2O$), and 624 ($[M + Li - H_2O - HCHO]^+$) (a_2). However, ions that are characteristic to this subclass arise from the cleavages initiated by the α-hydroxyl group of the *N*-acyl chain [18] (Scheme **2**). The elimination of the fatty acyl substituent as an aldehyde yields a weak peak of *m/z* 334 ion ($\underline{f}_{1b}$), corresponding to a lithiated *N*-formylsphingosine (Scheme **2a**, route f_1). This elimination is consistent with the observation of a lithiated aldehyde at *m/z* 345 ($[C_{22}H_{45}CHO + Li]^+$) ($\underline{c}_{3a'}$), which is diagnostic to the fatty acyl chain of this subclass. The prior formation of the lithiated *N*-formylsphingosine ion of *m/z* 334 ($\underline{f}_{1b}$) to the *m/z* 316 ion is reasoned by the fact that the *m/z* 286 and 298 ions were also observed in the spectrum. The *m/z* 316 is probably a lithiated oxetane or a lithiated aziridine ion arising from a H_2O loss from *m/z* 334 via the similar fragmentation processes as described earlier (Scheme **2a**). The oxetane ion of *m/z* 316 ($\underline{f}_{2b}$) dissociates to the *m/z* 286 ion ($\underline{f}_{3b}$) by loss of HCHO (route $f_{1a'}$). The aziridine ion of *m/z* 316 ($\underline{f}_{2b'}$) undergoes another H_2O loss to give the *m/z* 298 ($\underline{f}_{3b'}$) (route $f_{1b'}$).

The bond cleavage facilitated by the α-hydroxyl of the *N*-acyl chain is further evidenced by the presence of a base peak of *m/z* 306, arising from a combined losses of CO and $C_{22}H_{45}CHO$ from *m/z* 672 (Scheme **2b**, route e_1) [18]. This fragmentation pathway is consistent with the observation of the analogous ion of *m/z* 310 ion arising from the d_4-d18:1/h24:0-Cer at m/z 676 (Figure 4b). The *m/z* 306 ($[M + Li]^+ - CO - C_{22}H_{45}CHO$) ($\underline{e}_{1b}$) ion is a lithiated sphingosine ion, which undergoes further fragmentations by the same pathways as described in Scheme **1c**. This is supported by the product-ion spectrum of d_4-d18:1/h24:0-Cer (Figure 4b), in which the analogous ions resulting from further dissociations of the *m/z* 310 ion have a two-unit mass shift, consistent with the suggested mechanism (Scheme **2b**).

Ions that identify the h24:0 fatty acyl substituent were observed at *m/z* 416 ($\underline{c}_{2a}$) and 390 ($\underline{d}_{1a}$), analogous to those observed for *N*-acylsphingosines. Because of the presence of the α-hydroxyl group, the *m/z* 416 ion may dissociate into the lithiated aldehyde ion at *m/z* 345 ($\underline{c}_{3a'}$), by elimination of CO and $HNCH_2CH_2$ simultaneously (Scheme **2c**). This elimination is consistent with the observation of a lithiated aziridine ($[HNCH_2CH_2 + Li]^+$) at *m/z* 50, which is only observed for this subclass (Figure 4a, b, c, d, e, and f). A weak ion probably arising from further dissociation of *m/z* 654 by expulsion of NH=CO and $C_{22}H_{45}CHO$ was observed at *m/z* 273 ($\underline{d}_{3b}$) (Scheme **2d**). However, an analogous ion of *m/z* 291 becomes the most prominent in the product-ion spectra of the lithiated t18:0/hFA-Cer (discussed later). The proposed pathways for the fragmentations (Scheme **2**) are further supported by the product-ion spectrum of the $[M + Li]^+$ ions of d_4-d18:1/h24:0-Cer at *m/z* 676 (Figure 4b), which yields the analogous ions with the expected mass shifts. A similar pattern of ions was also observed for the $[M + Li]^+$ ions of d17:1/h16:0-Cer (*m/z* 546, Figure 4c), and of d18:1/h16:0-Cer (*m/z* 560, Figure 4d). The α-hydroxypalmitoyl moiety of the two compounds is reflected by the prominent ion at *m/z* 233 ($\underline{c}_{3a'}$), and the presence of the *m/z* 304 ($\underline{c}_{2a}$) and 278 ($\underline{d}_{1a}$) ions in the mass spectra. The 17:1-LCB of the former is identified by the prominent ions of *m/z* 292 ($\underline{e}_{1b}$), 284 ($\underline{f}_{3b'}$), 274 ($\underline{e}_{2b} + \underline{e}_{2b'}$), and 244 ($\underline{e}_{3b}$) along with the presence of the ions at *m/z* 250 ($\underline{e}_{3b''}$) and 302 ($\underline{f}_{2b} + \underline{f}_{2b'}$). The latter spectrum contains ions at *m/z* 306 ($\underline{e}_{1b}$), 298 ($\underline{f}_{3b'}$), 288 ($\underline{e}_{2b} + \underline{e}_{2b'}$), 258 ($\underline{e}_{3b}$), *m/z* 264 ($\underline{e}_{3b''}$), and 316 ($\underline{f}_{2b} + \underline{f}_{2b'}$), which are 14 Da higher and are diagnostic ions for *N*-α-hydroxyacylsphingosines.

As described earlier, the saturation of the LCB in the *N*-α-acylsphinganines results in the decline of the $\underline{a}_2$ ($[M + Li - H_2O - HCHO]^+$), $\underline{e}_{3b}$, $\underline{e}_{3b'}$ and $\underline{e}_{3b''}$ ions. These features are also observed for *N*-α-hydroxyacylsphinganines, and permit their distinction from *N*-α-hydroxyacylsphingosines. This is exemplified by the product-ion spectra of the $[M + Li]^+$ ions of d18:0/h16:0-Cer at *m/z* 562 (Figure 4e), and of d17:0/h16:0 at *m/z* 548 (Figure 4f). The *m/z* 514 ($\underline{a}_2$) and 260 ($\underline{e}_{3b}$) ions are of low abundance and ions at *m/z* 266 ($\underline{e}_{3b''}$) and 272 ($\underline{e}_{3b'}$) are absent in the spectrum of the former (Figure 4e). A similar result was also observed for the analogous ions of *m/z* 500 ($\underline{a}_2$), 246 ($\underline{e}_{3b}$), 252 ($\underline{e}_{3b''}$), and 258 ($\underline{e}_{3b'}$) in the

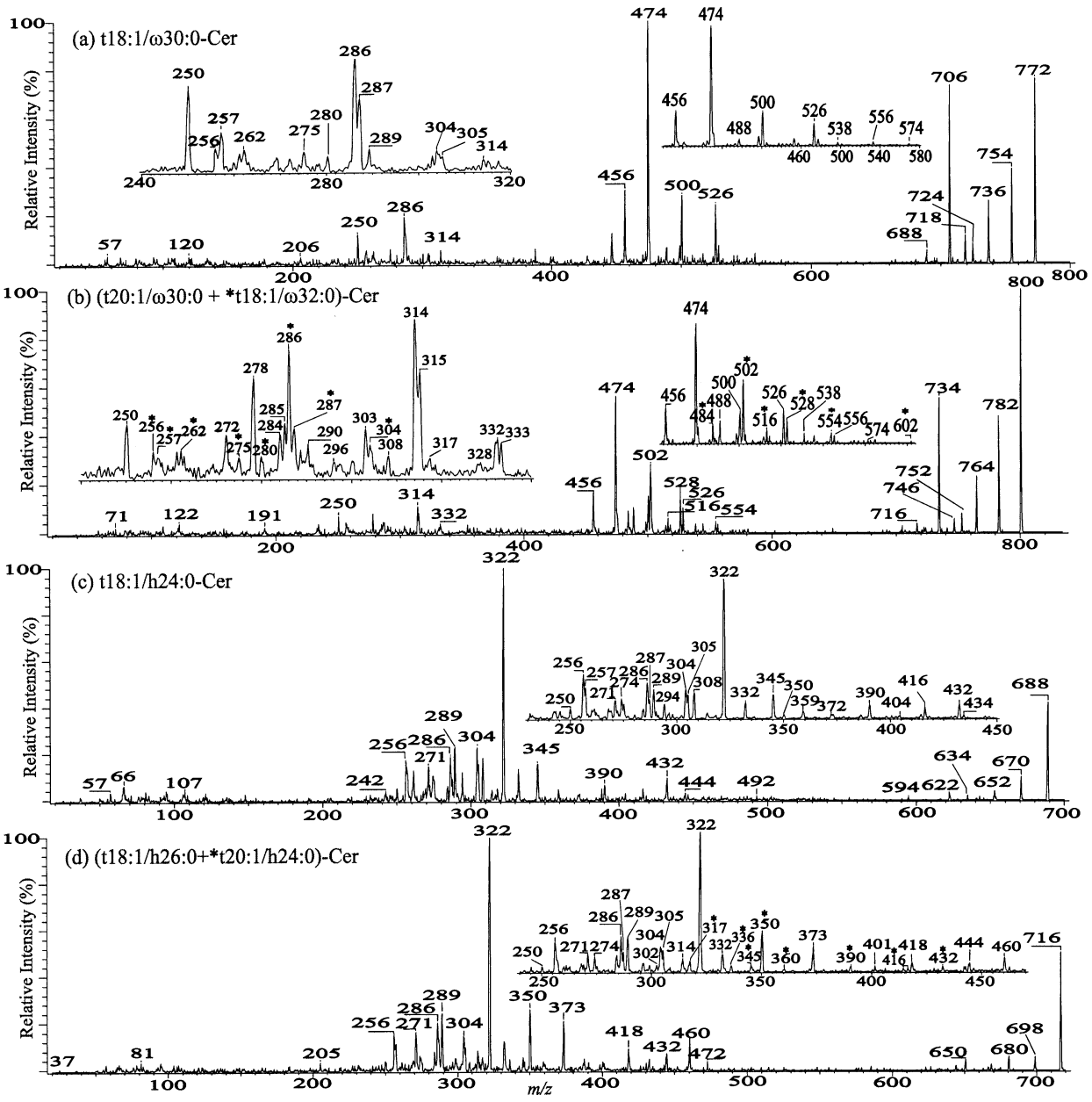

Figure 6. The product-ion spectra of the $[M + Li]^+$ ions of (**a**) t18:1/ω30:0-Cer at *m/z* 772, (**b**) (t20:1/ω30:0 + *t18:1/ω32:0)-Cer at *m/z* 800, (**c**) t18:1/h24:0-Cer at *m/z* 688, and of (**d**) (t18:1/h26:0 + *t20:1/h24:0)-Cer at *m/z* 716. Again, the presence of the α-hydroxy group in fatty acyl moiety (panels **c** and **d**) facilitates the fragmentations. The ions arising from the minor isomeric species are marked with an asterisk.

latter spectrum (Figure 4f). The low abundance of the $\underline{a}_2$ ion observed for the two spectra is also consistent with the decline of *m/z* 37, a $[HCHO + Li]^+$ ion.

While the $[M + Li]^+$ ions of d18:1/hFA-Cer undergo vigorous fragmentations because of the presence of the α-hydroxyl in the fatty acid substituent, the d18:1/ωFA-Cer undergoes fragmentations similar to that described for d18:1/nFA-Cer. This is illustrated by the product-ion spectrum of the $[M + Li]^+$ ions of d18:1/ω30:0-Cer at *m/z* 756 (Figure 4g). The identity of the ω-hydroxy fatty acyl substituent of the compound is revealed by the presence of the prominent ions at *m/z* 500 ($\underline{c}_{2a}$), 474 ($\underline{d}_{1a}$), and 456 ($\underline{d}_{2a}$). These ions are more abundant than the analogous ions observed for d18:1/nFA-Cer, attributable to the ω-hydroxyl group in the fatty acid substituent. In contrast, the ions at *m/z* 264 ($\underline{e}_{3b''}$), *m/z* 289 ($\underline{d}_{1b}$+ $\underline{d}_{1b'}$), 288 ($\underline{e}_{2b}$ + $\underline{e}_{2b'}$), 259 ($\underline{d}_{2b'}$) 258 ($\underline{e}_{3b}$), 282 ($\underline{e}_{4b'}$), 270 ($\underline{e}_{3b'}$), 271 ($\underline{d}_{2b}$), and 245 ($\underline{c}_{1b}$) that identify the d18:1-LCB are less abundant than the same ions observed for d18:1/nFA-Cer. A similar pattern of ions was observed for the lithiated d20:1/ω30:0-Cer at *m/z* 784 (Figure 4h), which is also composed of a minor d18:1/

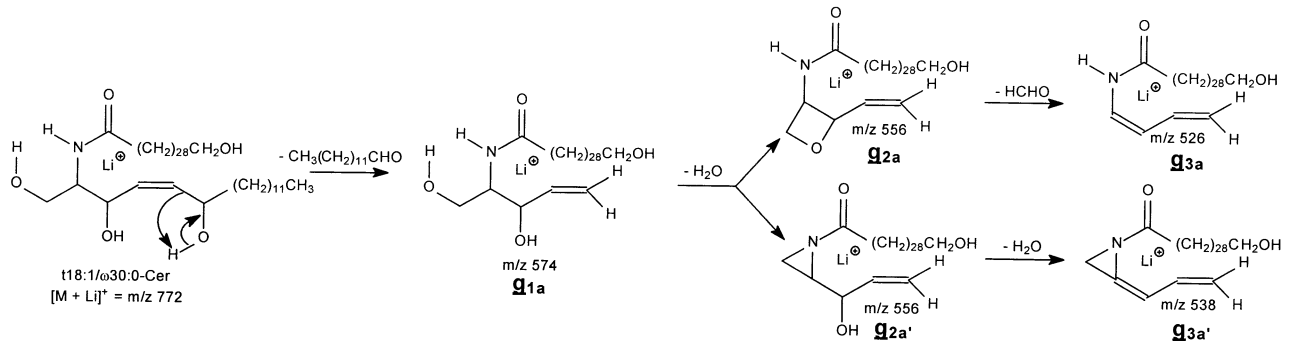

Scheme 4

ω32:0-Cer isomer. The d20:1/ω30:0-Cer component is identified by the prominent ions of 292 ($\underline{e}_{3b''}$), 298 ($\underline{e}_{3b'}$), 299 ($\underline{d}_{2b}$), 316 ($\underline{e}_{2b}$ + $\underline{e}_{2b'}$), and 273 ($\underline{c}_{1b}$), reflecting the d20:1-LCB, in combination with ions at *m/z* 500 ($\underline{c}_{2a}$), 474 ($\underline{d}_{1a}$), and 456 ($\underline{d}_{2a}$), which reflect the ω30:0-FA, whereas the d18:1/ω32:0-Cer isomer is identified by the presence of the *m/z* 528 ($\underline{c}_{2a}$), 502 ($\underline{d}_{1a}$), 484 ($\underline{d}_{2a}$), 264 ($\underline{e}_{3b''}$), 288 ($\underline{e}_{2b}$ + $\underline{e}_{2b'}$), and the 245 ($\underline{c}_{1b}$) ions in the spectrum.

N-acyl-4-hydroxysphinganine (N-acylphytosphingosine) and N-α-hydroxyacyl-4-hydroxysphinganine (N-α-hydroxyacylphytosphingosine)

As shown in Figure 5a, the $[M + Li]^+$ ion of *N*-tetradodecanoylphytosphingosine (t18:0/24:0-Cer) at *m/z* 674 yields a product-ion spectrum distinguishable from that obtained from the sphingosine subclass. The $\underline{a}_1$, $\underline{a}_2$, ($\underline{a}_1 - H_2O$), and ($\underline{a}_2 - H_2O$) series ions at *m/z* 656, 626, 638, and 608 are abundant, and the $\underline{a}_2$ ion of *m/z* 626 (656 − HCHO,) is less abundant than its precursor ion at *m/z* 656, a reversal from that observed for d18:1/nFA-Cer (Figure 1a, b, c, and d). This is consistent with the fact that the $\underline{a}_2$ ion from d18:1/nFA-Cer possesses an additional double bond at C-4 of the LCB and results in a conjugated bond, which is stable. Another feature in the product-ion spectra of this subclass is that the ($\underline{a}_2 - H_2O$) ion at *m/z* 608 is also abundant. This is attributed to the fact that the additional hydroxyl group at C-4 of the LCB, can participate in an additional H_2O loss and results in a stable conjugated ion, which is analogous to the $\underline{a}_2$ ion observed for d18:1/nFA-Cer.

Several prominent ions unique to this subclass were observed at *m/z* 428 ($\underline{b}_{1a}$) and 416 ($\underline{b}_{1b}$). The *m/z* 428 ion ($\underline{b}_{1a}$) may arise from the lithiated aziridine intermediate of *m/z* 656 ($\underline{b}_1$), by cleaving the C–C bond of the 3,4-diol of the LCB (Scheme **3**). This cleavage also results in a weak ion at *m/z* 233, corresponding to a lithiated aldehyde ($[C_{14}H_{29}CHO + Li]^+$). Another proposed pathway for formation of the *m/z* 428 ion involves a primary cleavage of the same bond of the lithiated t18:0/24:0-Cer ion of *m/z* 674 to a *m/z* 446 intermediate (not seen) by loss of an aldehyde and H_2, followed by a H_2O or HCHO loss to yield the *m/z* 428 or 416 ion (Scheme **3**). The observation of the above two ions, plus the ions at *m/z* 400 ($\underline{c}_{2a}$), 374 ($\underline{d}_{1a}$), and 356 ($\underline{d}_{2a}$) (Scheme **1b**), commonly observed for 24:0-FA, easily identifies the fatty acyl constituent of the molecule, whereas the identity of the phytosphingosine can be determined by the presence of the *m/z* 288 ($\underline{e}_{3b'}$), 289 ($\underline{d}_{2b}$), 263 ($\underline{c}_{1b}$), 307 ($\underline{d}_{1b}$+ $\underline{d}_{1b'}$), and 306 ($\underline{e}_{2b}$ + $\underline{e}_{2b'}$) ions. In the same spectrum, a set of the masses at *m/z* 442, 430, 414, 388, and 370, which reflect the 25:0-FA (the masses are 14-Da higher than the corresponding ions arising from 24:0-FA) were also observed, along with ions at *m/z* 274 ($\underline{e}_{3b'}$), 275 ($\underline{d}_{2b}$), 293 ($\underline{d}_{1b}$+ $\underline{d}_{1b'}$), and 249 ($\underline{c}_{1b}$), arising from t17:0-LCB. These ions clearly demonstrate that the lithiated molecular species of *m/z* 674 also contains a t17:0/25:0-Cer isomer. A minor t16:0/26:0-Cer isomer is also present in the spectrum. This is revealed by the masses of *m/z* 456, 444, 428 (overlap with the $\underline{b}_{1a}$ ions from t18:0/24:0-Cer), 402, and 384, which reflect the 26:0-FA and the masses that reflect the t16:0-LCB at *m/z* 235 ($\underline{c}_{1b}$), 260 ($\underline{e}_{3b'}$), and 261 ($\underline{d}_{2b}$). Figure 5b illustrates the product-ion spectrum of the *m/z* 660 ion, which also contains two sets of the ions arising from a major lithiated t17:0/24:0-Cer species and from a minor component of t16:0/25:0-Cer.

The concept that the α-hydroxyl group in the *N*-acyl chain facilitates the decompositions of ceramides is further evidenced by the product-ion spectra of *N*-α-hydroxyacylphytosphingosines. As illustrated in Figure 5c, the product-ion spectrum of the $[M + Li]^+$ ion of *N*-α-hydroxypalmitoylphytosphingosine (t18:0/h16:0-Cer) at *m/z* 578 contains weak ions at *m/z* 560 ($[M + Li - H_2O]^+$) ($\underline{a}_1$), 542 ($[M + Li - 2H_2O]^+$) ($\underline{a}_1 - H_2O$), and 530 ($[M + Li - H_2O - HCHO]^+$) ($\underline{a}_2$). The *m/z* 304 ($\underline{c}_{2a}$) and 233 ($\underline{c}_{3a'}$) ions that reflect the h16:0-FA, are of low abundance. In contrast, the analogous ions observed in the spectra of *N*-tetradodecanoylphytosphingosine are among the most prominent (Figure 5a and b).

The major fragmentation pathways for the lithiated t18:0/h16:0-Cer appear to arise from cleavage of the amide N–CO bond, resulting in a prominent ion at *m/z* 324 ($[M + Li]^+ - CO - C_{14}H_{29}CHO$) ($\underline{e}_{1b}$). This is followed by a H_2O loss to yield an aziridine ($\underline{e}_{2b'}$) or an oxetane ($\underline{e}_{2b}$) ion at *m/z* 306, which successively eliminates H_2O or HCHO to form the *m/z* 288 ($\underline{e}_{3b'}$) or *m/z* 276

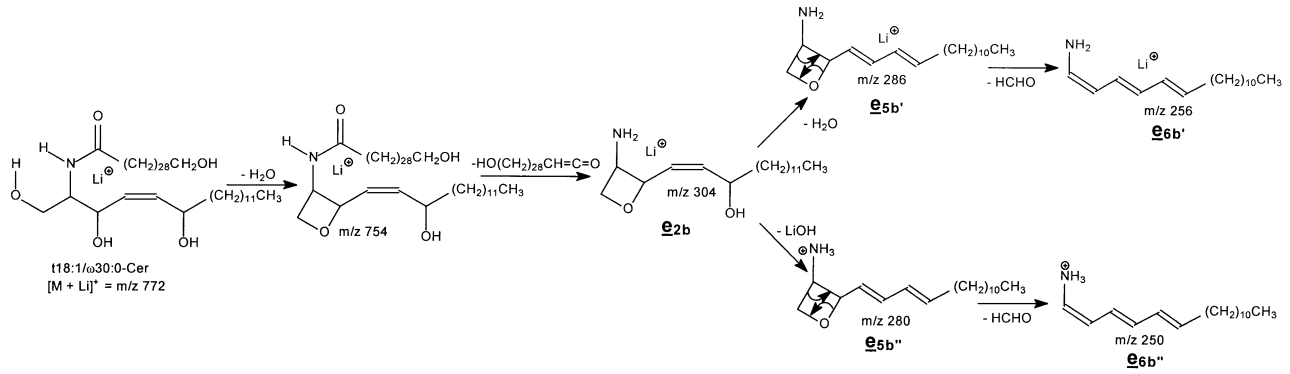

Scheme 5

($\underline{e}_{3b}$) ion, respectively. The ions at *m/z* 352 ($[M + Li]^+ - C_{14}H_{29}CHO$) ($\underline{f}_{1b}$), *m/z* 334 ($\underline{f}_{1b} - H_2O$) ($\underline{f}_{2b} + \underline{f}_{2b'}$), *m/z* 316 ($\underline{f}_{2b} - H_2O$) ($\underline{f}_{3b'}$), and *m/z* 304 ($\underline{f}_{2b'} -$ HCHO) ($\underline{f}_{3b}$) arise from the same pathways as described for *N*-α-hydroxyacylsphingosines (Scheme **2a**). Two sets of the masses analogous to the above ions were observed in the product-ion spectrum of *m/z* 564 (Figure 5d). The major isomer of t17:0/h16:0-Cer is identified by the presence of the *m/z* 304 ($\underline{c}_{2a}$) and 233 ($\underline{c}_{3a'}$) ions, reflecting the h16:0-FA, together with ions at *m/z* 338 ($\underline{f}_{1b}$), 320 ($\underline{f}_{2b} + \underline{f}_{2b'}$), 310 ($\underline{e}_{1b}$), 293 ($\underline{d}_{1b} + \underline{d}_{1b'}$), 292 ($\underline{e}_{2b'} + \underline{e}_{2b}$), 277 ($\underline{d}_{3b}$), 259 ($\underline{d}_{3b} - H_2O$), and 249 ($\underline{c}_{1b}$) that are unique to t17:0-LCB. The minor species of the t18:0/h15:0-Cer isomer is recognized by the major ions at *m/z* 352 ($\underline{f}_{1b}$), 334 ($\underline{f}_{2b} + \underline{f}_{2b'}$), 324 ($\underline{e}_{1b}$), 291($\underline{d}_{3b}$), and 219 ($\underline{c}_{3a'}$).

The apparent distinction among the product-ion spectra of the lithiated *N*-α-hydroxyacylsphingosines (Figure 4a, b and d) and *N*-α-hydroxyacylphytosphingosines (Figure 5c, d) lies on the fact that the $\underline{d}_{3b}$ series ion at *m/z* 273 for the former compounds is of low abundance, while the analogous ions at *m/z* 291 observed for t18:0/h16:0-Cer (Figure 5c) and at *m/z* 277 observed for t17:0/h16:0-Cer (Figure 5d) are the most prominent. When subjected to CAD, the $\underline{d}_{3b}$ series ions of *m/z* 273 and 291 undergo further loss of H_2O or HCHO (data not shown). The prominence of the $\underline{d}_{3b}$ ions observed for the *N*-α-hydroxyacylphytosphingosines but not for the *N*-α-hydroxyacylsphingosines may indicate that further fragmentation of the $\underline{d}_{3b}$ ion from the *N*-α-hydroxyacylphytosphingosines is thermodynamically less favorable than that from the *N*-α-hydroxyacylsphingosines, which possess an unsaturated LCB. An analogous ion was also observed for all the ceramides with a saturated LCB that have been examined. These include the *m/z* 291, 277, 275, and 261 ions in the product-ion spectrum of t18:0/24:0-Cer (Figure 5a), t17:0/24:0-Cer (Figure 5b), d18:0/h16:0-Cer (Figure 4e) and of d17:0/h16:0-Cer (Figure 4f), respectively. The analogous ions, however, were of low abundance in the product-ion spectra of all the *N*-acyl-4-sphingenine ceramides examined.

N-ω-hydroxyacyl-6-hydroxysphing-4-enine (t18:1/ωFA-Cer) and N-α-hydroxy-6-hydroxysphing-4-enine (t18:1/hFA-Cer)

The *N*-ω-hydroxyacyl-6-hydroxy-4-sphingenine (t18:1/ωFA-Cer) is a protein-bound ceramide found in human stratum corneum, whereas the *N*-α-hydroxy-6-hydroxysphing-4-enine (t18:1/hFA-Cer) is not protein bounded. The major species of the t18:1/ωFA-Cer found in human stratum corneum is t18:1/ω30:0-Cer [6], which gives the $[M + Li]^+$ ions at *m/z* 772 when subjected to ESI analysis. Upon CAD, the *m/z* 772 ion yields intense fragment ions at *m/z* 754 ($772 - H_2O$), 736 ($772 - 2H_2O$), and 718 ($772 - 3H_2O$), by consecutive losses of H_2O. Ions at *m/z* 724 (754 − HCHO), 706 (736 − HCHO), and 688 (718 − HCHO) probably arise from further loss of HCHO from *m/z* 754, 736, and 718, respectively (Figure 6a). The *m/z* 688 ion can also arise from an additional H_2O loss from the *m/z* 706 ion. This H_2O loss possibly eliminates the ω-hydroxyl of the fatty acid substituent. The ω-hydroxytriacontanoic acid moiety (ω30:0) was identified by the presence of the prominent ions at *m/z* 500 ($\underline{c}_{2a}$), 526 ($\underline{g}_{3a}$), 474 ($\underline{d}_{1a}$), and 456 ($\underline{d}_{2a}$), which are also abundant in the spectra of d18:1/ω30:0-Cer (Figure 4g) and d20:1/ω30:0-Cer (Figure 4h). The ions specific to this subclass arise from the decompositions initiated by the cleavage of C5–C6 bond of the LCB to a *m/z* 574 ($\underline{g}_{1a}$) ion, by eliminating an aldehyde (Scheme **4**). This is followed by a water loss step as described earlier, to yield both a lithiated oxetane ($\underline{g}_{2a}$) and aziridine ($\underline{g}_{2a'}$) intermediate at *m/z* 556, which dissociates to ions of *m/z* 526 ($\underline{g}_{3a}$) and 538 ($\underline{g}_{3a'}$) by explusion of HCHO and H_2O, respectively. The t18:1-LCB is recognized by the prominent $\underline{e}_{3b'}$ ion of *m/z* 286, which arises from *m/z* 754 ($[M + Li - H_2O]^+$) ($\underline{a}_1$) by the initial loss of the ω-hydroxyl fatty acid as a ketene (loss of $HO(CH_2)_{28}CH{=}C{=}O$) to yield the *m/z* 304 ion, probably a lithiated oxetane. This is followed by a H_2O or a LiOH loss to yield the *m/z* 286 ($\underline{e}_{5b'}$) or *m/z* 280 ($\underline{e}_{5b''}$) ion, respectively (Scheme **5**). These fragmentation processes also result in the *m/z* 256 ($\underline{e}_{6b'}$) and *m/z* 250 ($\underline{e}_{6b''}$) ions by further expulsion of HCHO and are consistent with the idea that a lithiated oxetane intermediate was primarily formed as described earlier.

Table 2. Minor fragment ions observed for various ceramide standards

Ceramide species			Fragment ions from CAD of $[M + Li]^+$																	
			common ions (*m/z*)		FA ions (*m/z*)				LCB ions (*m/z*)											
$[M + Li]^+$ (*m/z*)	Fatty acid	LCB	$\underline{a}_2$-H_2O	$\underline{a}_2$-LiOH	$\underline{c}_{1a}$	$\underline{g}_{1a}$	$\underline{g}_{2a} + \underline{g}_{2a'}$	$\underline{g}_{3a'}$	$\underline{c}_{1b}$	$\underline{d}_{1b} + \underline{d}_{1b'}$	$\underline{d}_{2b}$	$\underline{d}_{2b'}$	$\underline{d}_{3b}$-H_2O	$\underline{e}_{4b'}$	$\underline{e}_{3b}$	$\underline{f}_{1b}$	$\underline{f}_{3b}$	$\underline{f}_{2b} + \underline{f}_{2b'}$	$\underline{e}_{6b'}$	$\underline{e}_{6b''}$
656	24:0	d18:1			418				245	289[d]	271[d]	259		282	258					
654	24:1	d18:1			416				245	289[d]	271[d]	259		282	258					
657	24:1	d_3-d18:1			419				245	290[d]	271[d]	260		284	259					
432	8:0	d18:1	366	360	194				245	289[d]	271[d]	259		282	258					
544	16:0	d18:1	478	472	306				245	289[d]	271[d]	259		282	258					
572	18:0	d18:1	506	500	334				245	289[d]	271[d]	259		282	258					
658	24:0	d18:0	592	586	418				247[d]	291[d]	273[d]	261		284						
661	24:0	d_3-d18:0	593	586	419				247[d]	292[d]	273[d]	262		286						
574	18:0	d18:0	508	502	334				247[d]	291[d]	273[d]	261		284						
672	h24:0	d18:1	606						245	289	271				258[d]	334	286	316		
676	d_1-h24:0	d_3-d18:1	607						245	291	271				260[d]	338	288	318		
670	h24:1	d18:1	604						245	289	271				258[d]	334	286	316		
532	h16:0	d16:1	466						217	261	243				230[d]	306	258	288		
546	h16:0	d17:1	480						231	275	257				244[d]	320	272	302		
560	h16:0	d18:1	494						245	289	271				258[d]	334	286	316		
562	h16:0	d18:0	496						247	291	273				260	336	288	318[d]		
590	h18:0	d18:0	524						247	291	273				260	336	288	318[d]		
548	h16:0	d17:0	482						233	277	259				246	322	274	304[d]		
756	ω30:0	d18:1	690						245	289	271	259		282	258					
784	ω30:0	d20:1	718						273	317	299	287		310	286					
	ω32:0	d18:1	718						245	289	271	259		282	258					
578	h16:0	t18:0	512						263	307	289		273[d]		276	352	304	334		
564	h16:0	t17:0	498						249	293	275		259[d]		262	338	290	320		
800	ω30:0	t20:1	734			574	556	538	289	333	315	303							284	278[d]
	ω32:0	t18:1	734			602	584	566	261	305	287	275							256	250[d]
772	ω30:0	t18:1	706			574	556	538	261	305	287	275							256	250[d]
744	ω28:0	t18:1	678			546	528	510	261	305	287	275							256	250[d]
674	24:0	t18:0	608						263[d]	307	289[d]			282						
	25:0	t17:0	608						249[d]	293	275[d]			268						
	25:0	t17:0	608						235[d]	279	261[d]			254						
660	24:0	t17:0	594						249[d]	293	275[d]			268						
702	26:0	t18:0	636						263[d]	307	289[d]			282						
688	h24:0	t18:1	622						261	305	287[d]		271[d]		274	350	302	332[d]	256[d]	250
716	h26:0	t18:1	650						261	305	287[d]		271[d]		274	350	302	332[d]	256[d]	250

[d]diagnostic ions.

Therefore, ceramides with a t18:1-LCB can be easily recognized by the presence of *m/z* 250, 256, 280, and 286 in addition to ions at *m/z* 305 ($\underline{d}_{1b}$ + $\underline{d}_{1b'}$), 287 ($\underline{d}_{2b}$), 304 ($\underline{e}_{2b}$ + $\underline{e}_{2b'}$), 275 ($\underline{d}_{2b'}$), and 289 ($\underline{d}_{3b}$). Figure 6b illustrates the product-ion spectrum of *m/z* 800, which contains two sets of the feature ions that identify both a t20:1/ω30:0-Cer and a t18:1/ω32:0-Cer isomer.

The subclass of t18:1/hFA-Cer found in human stratum corneum is mainly composed of t18:1/h24:0-Cer and t18:1/h26:0-Cer [5], which yields the lithiated molecular species at *m/z* 688 and 716, respectively, by ESI. Both the $[M + Li]^+$ ions of t18:1/h24:0-Cer at *m/z* 688 (Figure 6c) and of the t18:1/h26:0-Cer at *m/z* 716 (Figure 6d) undergo vigorous fragmentation when subjected to CAD. This is attributable to the presence of the α-hydroxyl group in the fatty acyl substituent of the molecule, as observed earlier. The major ions may arise from the same fragmentation pathways as described in Scheme **2**. The fragment ions and the assignment of the ion species observed for the two ceramides after CAD are shown in Tables 1 and 2. The product-ion spectrum of t18:1/h24:0-Cer at *m/z* 688 (Figure 6c) is dominated by a prominent ion at *m/z* 322 ($\underline{e}_{1b}$), and ions at *m/z* 289 ($\underline{d}_{3b}$), 304 ($\underline{e}_{2b}$ + $\underline{e}_{2b'}$), and 286 ($\underline{e}_{3b'}$ + $\underline{e}_{5b'}$) that reflect the 6-hydroxysphing-4-enine LCB. The ions at *m/z* 345 ($\underline{c}_{3a'}$), 416 ($\underline{c}_{2a}$), and 390 ($\underline{d}_{1a}$) that reflect the h24:0 fatty acyl substituent are of low abundance. The product-ion spectrum of the t18:1/h26:0-Cer at *m/z* 716 (Figure 6d) is also dominated by the *m/z* 322 ion along with the above described ions that reflect the t18:1-LCB, whereas the h26:0 fatty acid substituent is revealed by ions at *m/z* 373 ($\underline{c}_{3a'}$), 444 ($\underline{c}_{2a}$), and 418 ($\underline{d}_{1a}$). The identification of the minor isomeric component in the same spectrum (Figure 6d) again is established by the second set of the diagnostic ions that reflect the t20:1-LCB and h24:0-FA. In contrast, the $[M + Li]^+$ ions of t18:1/ωFA-Cer (Figure 6a and b) undergo less fragmentation and the fragment ions are dominated by the ions reflecting the fatty acyl substituent.

Conclusions

Ceramides isolated from living organisms occur as complex mixture of different classes. For example, ceramides in human stratum corneum alone consist of at least eight subclasses [2–6], and even each ceramide class is a complex mixture of individual molecular species, which may consist of more than one isomer, as is revealed by the present method. Previous study by FAB in the structural characterization of ceramides using high-energy tandem mass spectrometry was limited in a small variety of ceramides and isomer differentiation among ceramide classes was not demonstrated [19]. This paper, for the first time as to our knowledge, reports an extensive study including a large variety of structurally diverse ceramides using low-energy CAD tandem mass spectrometry with ESI. Although the major fragment ions observed are similar to that reported by FAB high-energy CAD, some significant differences from the FAB method were observed: (1) The classical C–C bond cleavages arising from charge-remote fragmentation process were not present, and (2) ions arising from cleavage of the β–γ bond of the fatty acid substituent (K type ion) and from neutral loss of 240 (S type ion) and of 239 (S + 1 type ion) (for sphingosine LCB) are not observable [19]. However, the low-energy CAD tandem mass spectra obtained in this study contain multiple abundant fragment ions that reflect both the fatty acid and the LCB substituents of the molecules and thus, structural identification can be easily achieved. These features of the tandem mass spectra are especially useful for identification of isomeric structures in mixtures. This has been demonstrated in Figures 5 and 6, in which more than one isomer can be found. Other important findings are that the $\underline{a}_1$, $\underline{a}_2$, and ($\underline{a}_1 - 30$) ions (from consecutive losses of H_2O and HCHO), which are abundant in our study, are not present in the previous study by FAB [19]. These feature ions have been successfully used for screening ceramide in biological samples by tandem mass spectrometry [25].

The methods described here permit the structure of ceramides to be revealed in detail. The fragmentation pathways for the ion formations are similar to those reported for glycosphingolipids [24]. The application of this technique to the structural determination of an entire class of new 6-hydroxy-4-sphingenine containing ceramides in human skin is now in progress.

Acknowledgments

This research was supported by U.S. Public Health Service grants P41-RR-00954, R37-DK-34388, P60-DK-20579, and P01-HL-57-278 and grant 996003 from the Juvenile Diabetes Foundation.

References

1. Wertz, P. W.; Downing, D. T. Ceramides of Pig Epidermis: Structure Determination. *J. Lipid Res.* **1983,** *24,* 759–765.
2. Wertz, P. W.; Downing, D. T. Covalently Bound Hydroxyacylsphingosine in the Stratum Corneum. *Biochim. Biophys. Acta.* **1987,** *917,* 108–111.
3. Wertz, P. W.; Swartzendruber, D. C.; Madison, K. C.; Downing, D. T. Composition and Morphology of Epidermal Cyst Lipids. *J. Invest. Dermatol.* **1987,** *89,* 419–425.
4. Wertz, P. W.; Madison, K. C.; Downing, D. T. Covalently Bound Lipids of Human Stratum Corneum. *J. Invest. Dermatol.* **1989,** *92,* 109–111.
5. Robson, K. J.; Stewart, M. E.; Michelsen, S.; Lazo, N. D.; Downing, D. T. 6-Hydroxy-4-Sphingenine in Human Epidermal Ceramides. *J. Lipid Res.* **1994,** *35,* 2060–2068.
6. Stewart, M. E.; Downing, D. T. A New 6-Hydroxy-4-Sphingenine-Containing Ceramide in Human Skin. *J. Lipid Res.* **1999,** *40,* 1434–1439.
7. Hannun, Y. A.; Luberto, C. Ceramide in the Eukaryotic Stress Response. *Trends Cell Biol.* **2000,** *10,* 73–80.
8. Kolesnick, R. N.; Kronke, M. Regulation of Ceramide Production and Apoptosis. *Ann. Rev. Physiol.* **1998,** *60,* 643–665.
9. Okazaki, T.; Kondo, T.; Tashima, M. Diversity and Complexity of Ceramide Signaling in Apoptosis. *Cell Signal.* **1998,** *10,* 685–692.
10. Obeid, L. M.; Hannun, Y. A. Ceramide: A Stress Signal and Mediator of Growth Suppression and Apoptosis. *J. Cell Biochem.* **1995,** *58,* 191–198.

11. Fishbein, J. D.; Dobrowsky, R. T.; Bielawska, A.; Garrett, S.; Hannun, Y. A. Ceramide-Mediated Growth Inhibition and CAPP are Conserved in Saccharomyces cerevisiae. *J. Biol. Chem.* **1993,** *268,* 9255–9261.
12. Venable, M. E.; Lee, Y. L.; Smith, M. J.; Bielawska, A; Obeid, L. M. Role of Ceramide in Cellular Senescence. *J. Biol. Chem.* **1995,** *67,* 27–38.
13. Chao, M. V. Ceramide: A Potential Second Messenger in the Nervous System. *Mol. Cell Neurosci.* **1995,** *6((2)),* 91–96.
14. Cremesti, A. E.; Fischl, A. S. Current Methods for the Identification and Quantitation of Ceramides: An Overview. *Lipids* **2000,** *35,* 937–945 and references therein.
15. Sullards, M. C.; Merrill, A. H., Jr. Analysis of Sphingosine 1-Phosphate, Ceramides, and Other Bioactive Sphingolipids by High-Performance Liquid Chromatography-Tandem Mass Spectrometry. *Science's STKE* **2001**, 1–11 and references therein.
16. Liebisch, G.; Drobnik, W.; Reil, M.; Trumbach, B.; Arnecke, R.; Olgemoller, B.; Roscher, A.; Schmitz, G. Quantitative Measurement of Different Ceramide Species from Crude Cellular Extracts by Electrospray Ionization Tandem Mass Spectrometry (ESI-MS/MS). *J. Lipid Res.* **1999,** *40,* 1539–1546.
17. Gu, M.; Kerwin, J. L.; Watts, J. D.; Aebersold, R. Ceramide Profiling of Complex Lipid Mixtures by Electrospray Ionization Mass Spectrometry. *Anal. Biochem.* **1997,** *244,* 347–356.
18. Ann, Q.; Adams, J. Structural Determination of Ceramides and Neutral Glycosphingolipids by Collisional Activation of $[M + Li]^+$ ions. *J. Am. Soc. Mass Spectrom.* **1992,** *3,* 260–263.
19. Ann, Q.; Adams, J. Structural-Specific Collison-Induced Fragmentations of Ceramides Cationized with Alkaline-Metal Ions. *Anal. Chem.* **1993,** *65,* 7–13.
20. Costello, C. E., Vath, J. E. In *Methods in Enzymology*; McCloskey, J. A., Ed.; Academic Press: San Diego, CA, 1990; Vol CXCIII, pp 738–768.
21. Hsu, F.-F.; Turk, J. Structural Determination of Sphingomylin by Tandem Mass Spectrometry with Electrospray Ionization. *J. Am. Soc. Mass Spectrom.* **2000,** *11,* 437–449.
22. Adams, J.; Gross, M. L. Energy Requirements for Remote Charge Site Decompositions and Structural Information from Collisional Activation of Alkali Metal Cationized Fatty Alcohols. *J. Am. Chem. Soc.* **1988,** *108,* 6915–6921.
23. Hsu, F.-F., Turk, J. Characterization of Ceramides by Low Energy Collisional-Activated Dissociation Tandem Mass Spectrometry with Negative-Ion Electrospray Ionization. *J. Am. Soc. Mass Spectrom.* 2002, *13,* 558–570.
24. Hsu, F.-F.; Turk, J. Structural determination of Glycosphigolipids as Lithiated Adducts by Electrospray Ionization Mass Spectrometry Using Low-Energy Collisional-Activated Dissociation on a Triple Stage Quadrupole Instrument. *J. Am. Soc. Mass Spectrom.* **2001,** *12,* 61–79.
25. Hsu, F.-F., Turk, J., Stewart, M. E., Downing, D. T. Total Analysis of New 6-Hydroxy-4-Sphingenine-Containing Ceramides in Human Skin by ESI Tandem Mass Spectrometry, unpublished.